

Larry A. Franks, et. al.. "Radioactivity Measurement."

Copyright 2000 CRC Press LLC. <<http://www.engnetbase.com>>.

Radioactivity Measurement

Larry A. Franks

Sandia National Laboratories

Ralph B. James

Sandia National Laboratories

Larry S. Darken

Oxford Instruments, Inc.

- 66.1 Gaseous Detectors
General Operating Principles • Proportional Counters • Geiger-Müller Counters • Availability • Scintillation Detectors • Scintillation Process
 - 66.2 Germanium Detectors
Leakage Current • Coaxial Detectors • X-Ray Detection • Current Status of HPGe Detector Technology
 - 66.3 Silicon Detectors
Diffused Junction Detectors • Ion Implanted Detectors • Energy Resolution • Spatial Resolution • Present Status of Silicon Detector Technology
 - 66.4 Room-Temperature Semiconductors
Theory of Operation • Operational Considerations
 - 66.5 Prices and Availability
- References

Radioactivity was first discovered by Henry Becquerel in 1896 when he noticed that photographic plates became fogged after exposure to uranium atoms. In addition to uranium nuclei, many other naturally occurring and man-made isotopes are known to be radioactive and decay by emitting uncharged particles (gamma rays and neutrons) and charged particles (alpha or beta particles) from their nuclei. Over the past few decades, there has been a growing need for monitoring, locating, and imaging radioactive sources in a wide variety of medical, environmental, industrial, space, scientific, and national security applications. Many of the applications rely on the use of commercially available radiation detectors, whereas others require development of new detectors to meet system requirements related to sensitivity, power, size, portability, ruggedness, maintenance, radiation hardness, and energy resolution.

The signals generated by a radiation-sensing system depend on (a) the mechanisms in which the incident radiation interacts with the detector material and (b) the scheme used to readout the interaction. In general, there are three types of radiation sensors in use today: gas-filled detectors, scintillation devices, and semiconductor detectors. The types of radiation sensors can also be divided into two groups according to whether they can measure the energy of the emitted gamma-rays, X-rays, or charged particles. Whenever an energy-resolving capability is desired, a large number of information carriers must be generated for each absorbed pulse to reduce the statistical limit on energy resolution. This is best accomplished by use of semiconductor detectors, although some spectral information can be achieved through the use of scintillators and gas-filled detectors.

The typical unit of measure of radioactivity is the becquerel (Bq), which is defined as the rate of one disintegration per second of a decaying isotope. Another common measure of radioactivity is the curie, which can be obtained by multiplying the becquerel by 3.7×10^{10} .

This chapter is divided into sections on gaseous, scintillation, and semiconductor detectors. Separate sections describing semiconductor detectors that must be cooled to cryogenic temperatures for operation and those capable of operation at ambient temperatures are presented. There are several texts devoted to the subject of radiation detection [1–7], and the reader is directed to these books for more detailed information on the principles of detector operation, device performance, problems limiting detector performance, areas of current research and development, and applications.

66.1 Gaseous Detectors

Ionization in a gas resulting from the interaction of X and gamma radiation is the basis for a wide variety of radiation detectors. The versatility of gas phase detection arises from the great flexibility in detector sizes and shapes that can be produced, their relatively low production cost, and particularly, the ability to perform a multitude of measurement tasks. Gas detectors can be separated into three distinct types: ionization chambers, Geiger-Müller counters (tubes), and proportional counters with numerous variations of each type. All utilize the ions and electrons created by the interaction of an incident photon with the detector gas, directly or indirectly, to produce an output signal. They differ in the characteristics of the electric field and nature of the output signal.

Ionization chambers can be operated in either a current mode or pulsed mode, although the current mode is more common. They operate by collecting (with an applied electric field) all the charge generated by the original ionizing event and differ in this way from both proportional and Geiger-Müller counters. The latter, normally operated in a pulsed mode, have output signals that result from amplification of the original ion pairs by gas multiplication processes.

General Operating Principles

Fundamental to the operation of gas detectors is the generation of electron-ion pairs and their movement through the surrounding gas under the influence of an applied electric field. It is convenient to summarize basic features of these processes before turning to specific detector designs.

W Values

The energy (W) required to produce an electron-ion pair in a gas depends on the gas, the type of radiation (and its energy). W values for fast electrons in common filling gases range from 26.4 eV per ion pair in argon to 41.3 eV per ion pair in helium. The presence of nonionizing energy loss processes accounts for the W values greatly in excess of the ionization energy. Fluctuations in the number of pairs produced from photons of the same energy are of significance in pulse-mode operation. The variance is generally less than expected based on Poisson statistics and is accounted for by an empirical constant, the Fano factor (typically 0.1 to 0.2).

Charge Transport

The motion of free electrons and ions in the gas under the influence of the electric field (E) is quite different. The drift velocity (v) of the more massive ions is a linear function of E/p where p is the gas pressure. It can be expressed as

$$v = \frac{\mu E}{p} \quad (66.1)$$

The proportionally constant μ is the mobility, which depends on the type of gas and the charge of the ion. Values are typically in the region of 1000 cm²/V-s/mm Hg. The electron mobility is normally about 1000 times ion values; the electron drift velocity is not linear in E/p [8].

Electric Field Effects

The amplitude of a pulse resulting from the interaction of a photon with the wall or fill gas depends strongly on the voltage applied to the detector and serves to distinguish the three detector types. A plot of pulse amplitude as a function of applied voltage is shown in Figure 66.1. The plateau following the initial steep segment is the region of ion chamber operation. It is a region where the electric field is sufficient to reduce recombination of the original pairs to an acceptable value and further voltage increases yield no more charge (as it has all been collected) and ion saturation is established. Assuming complete charge collection, the output current accurately represents the rate ion pairs are being produced. This is the basis for ionization chamber operation.

The rapidly rising portion following the plateau marks the onset of gas multiplication (the initial electrons can acquire enough energy between collisions to generate further ionization). In the initial segment, the multiplication process is linear; that is, the charge collected is proportional to the number of original ion pairs. This is the defining characteristic of proportional counter operation. The proportionality eventually is ended at higher voltages by space charge effects caused by positive ions.

At yet higher voltages, the space charge becomes sufficient to reduce the electric field below the multiplication threshold and no further multiplication takes place. Thus, a condition is reached where the same number of positive ions are produced for all initial ion-pair populations, and the pulse amplitude is independent of the initial conditions. This characterizes Geiger-Müller counter operation.

Further details on the operation of these devices may be found in texts by Knoll [1], Price [9], Attix and Roesch [10], and Tait [11]. The monograph by Rossi and Staub [2] contains a lengthy discussion of ionization chambers together with data on the physics of the transport process.

Ionization Chambers

Ionization chambers have been designed for numerous X- and gamma-ray measurement applications. They are frequently employed in radiation survey instruments. They are found in parallel plate, cylin-

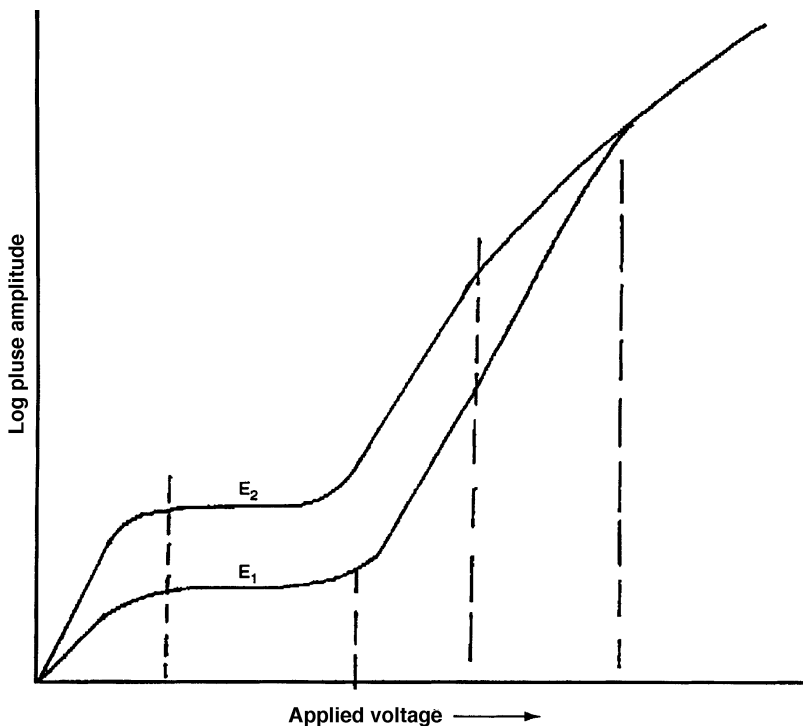


FIGURE 66.1 Distinct operating regions of gas-filled detectors. E_1 and E_2 depict pulses from photons of two energies.

drical, and spherical geometries. Essential features of their design can be found in the parallel plate chamber shown schematically in Figure 66.2. The design shown contains an optional guard ring that helps to define the active volume of the chamber. The ring is normally maintained near the collector electrode potential. (Guard rings are also employed in very low current designs to reduce leakage current.) Because the current for the ionization chamber is low, typically 1 nA or less, considerable care must be taken with the insulators to minimize leakage currents.¹

Because of the low output current, special care must be taken with the readout system. Both dc and dynamic-capacitor types are used. Only electrometers of the highest quality should be used. Dynamic-capacitor (or vibrating-reed) varieties provide more stable operation. They are normally the choice for very low current applications.

Several special-purpose ion chambers are notable. The “free air” chamber, a parallel-plate variant, is valued for accurate gamma ray exposure measurements, particularly when absolute measurements are required. This is achieved by collimation of the incoming gamma flux and by an internal design that ensures compensation for ionization produced outside the sensitive volume by secondary electrons. These chambers are limited to energies below about 100 keV, however. Cavity ionization chambers are widely used for dosimetry purpose. To function in this manner, it is necessary that they be designed to meet the requirement of the Bragg-Gray principle [12]. This states that the absorbed dose in a medium can be determined from the ionization produced in a small gas-filled cavity in the medium. The cavity dimension must be small compared to the range of the ionizing particles generated in the material so that the particle flux is essentially unperturbed. Of particular interest for health physics applications are

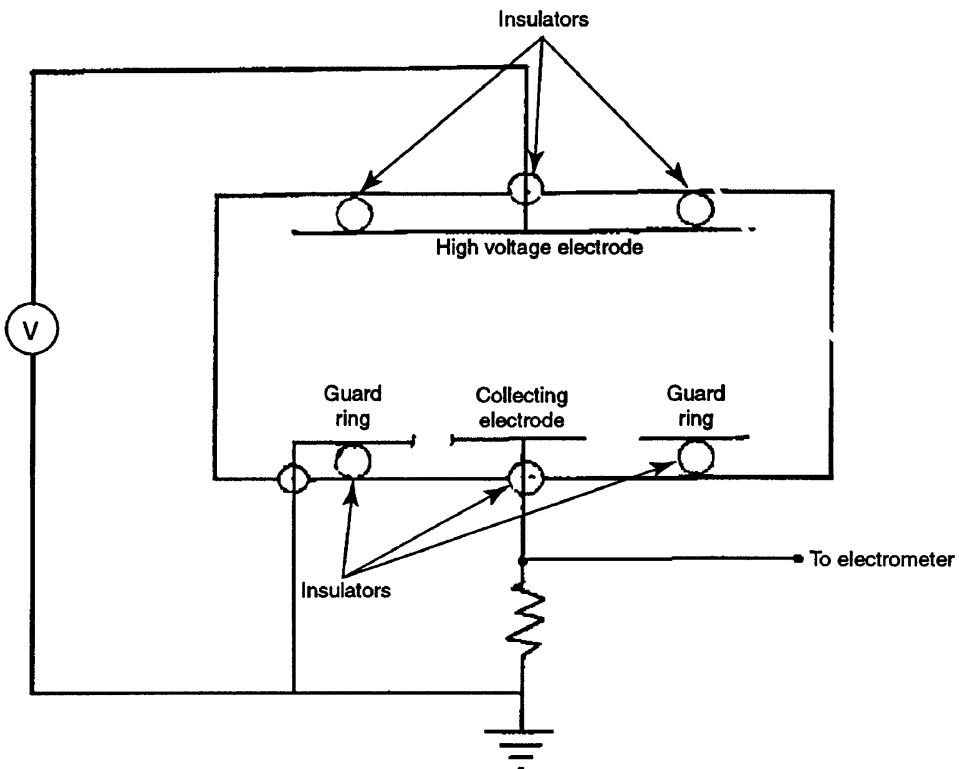


FIGURE 66.2 Schematic diagram of parallel-plate ionization chamber with guard ring defining active volume.

¹Note also that ionizing radiation can cause both permanent and transient resistivity losses in insulating materials and should be considered in high-flux or high-fluence applications.

tissue equivalent chambers where the wall material is a plastic that closely simulates the absorption properties of tissue.

Proportional Counters

Proportional counters utilize gas multiplication to amplify the charge of the initial ion pair population and have the important characteristic that the charge associated with the amplified pulse is proportional to the ion pairs produced initially. They are normally operated in a pulse mode. They can be operated sealed or in a gas flow mode. The sealed style is most common for X- and gamma-ray applications. While they are found in a number of geometries, cylindrical is the most common shape. A typical cylindrical design is shown in Figure 66.3. This relatively simple design features a central wire that is maintained at high voltage and a surrounding metal container that serves as the cathode. The electric field in this geometry is given by

$$E(r) = \frac{V}{r} \ln\left(\frac{b}{a}\right) \quad (66.2)$$

where V = anode-cathode voltage, a = anode wire radius, and b = inner radius of the cathode.

It should be noted that $E(r)$ depends on the diameter of the anode wire, allowing the threshold electric field needed for multiplication to be obtained at relatively modest voltages. The multiplication process is confined to a small volume surrounding the anode where the field exceeds the multiplication threshold. The characteristics of several common counting gases are given in Table 66.1.

TABLE 66.1 Characteristics of Common Proportional Counter Gases

Gas	W (eV per ion pair)	Fano Factor	Resolution (%) @ 5.9 keV	
			Calculated	Measured
Ne + 0.5% Ar	25.3	0.05	10.1	11.6
Ar + 0.5% C ₂ H ₂	20.3	0.075	9.8	12.2
Ar+ 10% CH ₄	26.0		12.8	13.2

Source: adapted from Knoll [1].

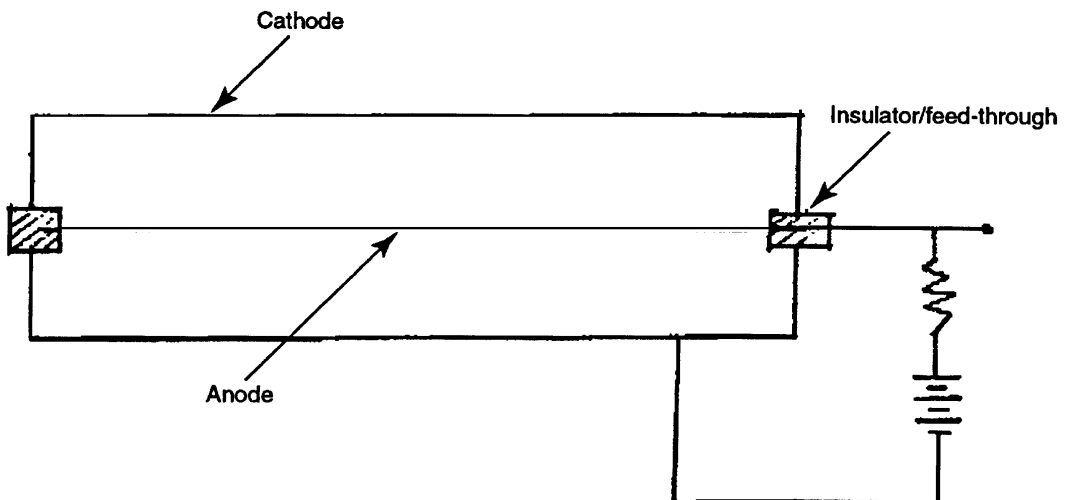


FIGURE 66.3 Schematic diagram of cylindrical proportional counter.

Proportional counters can be used for both photon and particle measurements. In photon applications they are particularly valued for spectroscopy in the low energy X-ray region. Their energy resolution and detection efficiency is generally inferior to semiconductor detectors such as lithium-drifted silicon or mercuric iodide but they offer large surface areas, reliable operation, and low cost. The energy resolution ΔE for given gas mixture for a specific photon energy can be estimated from the statistical limit given by

$$\Delta E = 2.35 \left[W \frac{(F + \beta)}{E} \right]^{1/2} \quad (66.3)$$

where F = Fano Factor, β = variance factor (typically about 0.5) [1], E = energy in eV, and W = energy in eV required to produce an ion pair.

Energy resolution for a proportional counter at 5.9 keV can be expected to be on the order of 10 percent (Table 66.1).

Geiger-Müller Counters

Geiger-Müller counters (more commonly known as G-M counters or tubes) remain among the most widely used means of detecting X and gamma radiation. They have high sensitivity, are rugged, and offer low cost. Also of importance is the large amplitude of the output pulse (several volts, typically), which greatly simplifies the readout. Because of these factors, they are the detectors of choice for a variety of commercial gamma survey instruments. Like proportional counters, they utilize gas amplification to generate an output pulse, although here the output is independent of the initial number of ion pairs. They are counters only and not applicable to spectroscopy. A G-M counter with typical readout is shown schematically in Figure 66.4.

G-M counters typically use a noble gas filling, most frequently argon or helium. The gas pressure is normally in the region of a few tenths of an atmosphere. At this pressure, a typical counter would require about 1000 V.

The process that terminates multiplication in a G-M counter has important counting implications. The positive ions space charge and resultant subthreshold electric field (for gas multiplication) persist for some time after the discharge is terminated. As a result, there is an interval following each pulse when pulses from subsequent input gamma rays are not produced or have less than full amplitude. This is

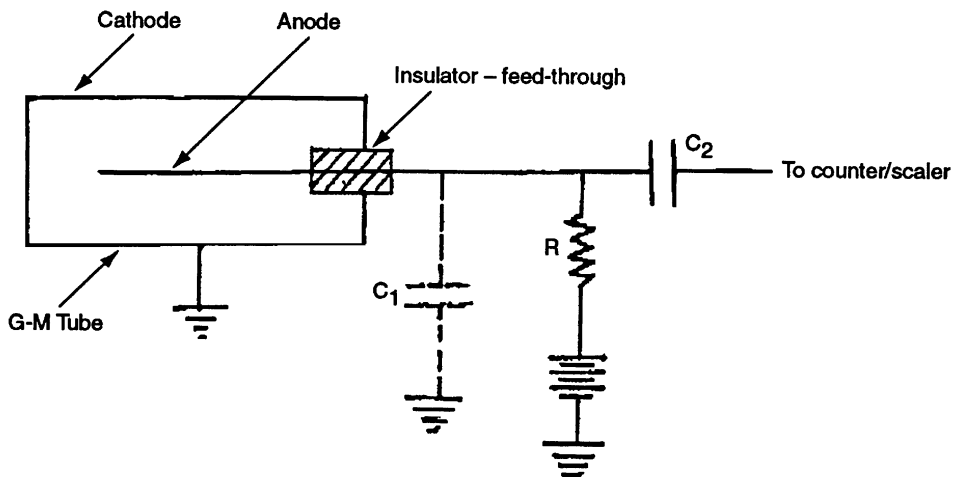


FIGURE 66.4 Typical counting circuit using a G-M tube. C_1 represents the combined tube and wiring capacitance, C_2 is a blocking capacitor that isolates the high voltage from the counter/scaler. The time constant of the circuit is RC_1 .

illustrated in Figure 66.5. The period between a full-amplitude pulse and the next discharge of any size is the dead time of the G-M counter (T_d). The time from the initial full amplitude pulse until another full amplitude pulse can be produced is the recovery time. Dead times in G-M counters are on the order of 100 μ s, with recovery time several times that. If the dead time is known and independent of count rate, the true count rate R_t may be determined in most cases from the observed rate R_o by the expression

$$R_t = \frac{R_o}{1 - R_o R_d} \quad (66.4)$$

Availability

Ionization chambers, Proportional counters, and Geiger-Müller counters are standard commercial products. They are available as stand-alone detectors requiring the user to supply ancillary electronics or as part of an instrument. Custom design devices are also available.

Scintillation Detectors

Scintillators, one of the oldest means of detecting gamma radiation, remain the method of choice for a multitude of counting and spectroscopy applications, particularly when counting efficiency rather than high-energy resolution is the primary objective. They are also widely used to record transient radiation events and in timing applications. While available in solid, liquid, and gas phases, solids and liquids are preferred for gamma-ray applications. Scintillators have the common property of converting energy absorbed from the incident gamma ray into visible or near visible light. The scintillation detector thus consists of a scintillator element, in which gamma ray energy is converted to optical photons, and some form of a photocell, normally a photomultiplier tube, to convert the optical photons into an electrical signal for processing by ancillary electronics.

Desired properties of a scintillator include high transparency to its own optical emission, efficient conversion of the absorbed gamma energy into optical output, short duration of the output, and output

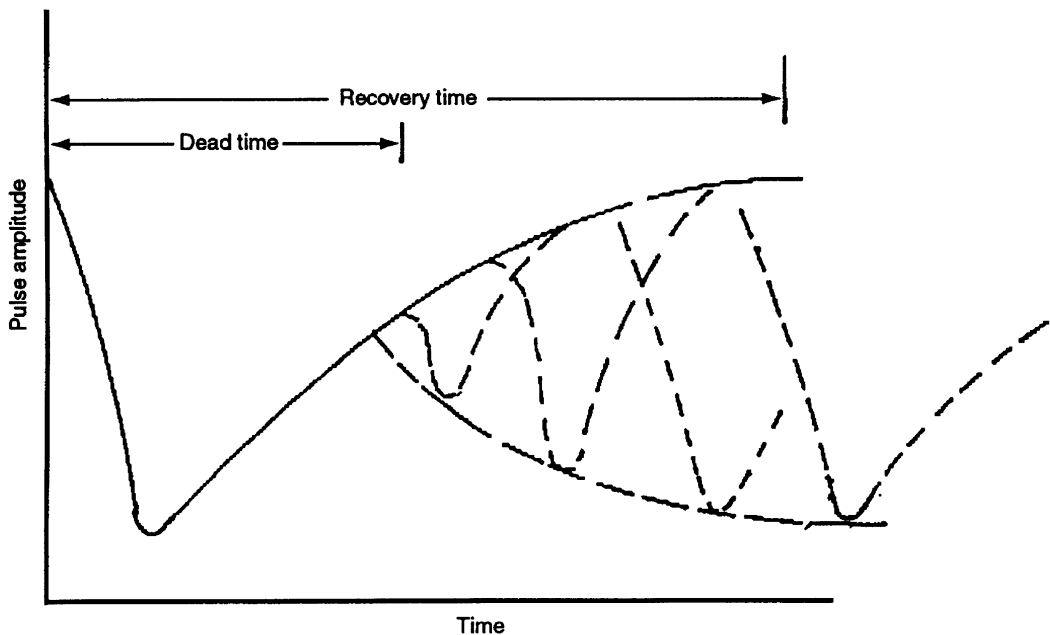


FIGURE 66.5 Illustration of dead time (T_d) in a typical G-M counter.

that is proportional to the amount of energy absorbed. Other useful properties include the ability to be produced in large sizes, ability to be machined, stable output over a wide range of environmental conditions, and efficient gamma-ray absorption.

Scintillation Process

The excess energy contained by the scintillator as a result of the gamma-ray absorption is dissipated largely through nonradiative processes and appears as heat. A small fraction decays radiatively and appears as visible and near visible light. That fraction of the absorbed energy converted to optical photons is referred to as the scintillation efficiency, which varies from <1 to ≈10 percent for the more efficient scintillators.

The optical emission originates from electronically excited atomic and molecular states. The emission is broadband, frequently exceeding 50 nm at the half-intensity points. Temporally, it is characterized by a very fast rise, followed by exponential decay. For most purposes, the light pulse can be adequately represented by

$$I(t) \propto N \left[e^{-\frac{t}{\tau}} - e^{-\frac{t}{\tau_R}} \right] \quad (66.5)$$

where $I(t)$ is intensity at time t , and N is related to the total number of scintillation photons. τ_R is the time constant associated with the pulse rise time, and τ is the time constant for decay. The time required for the intensity to fall to $1/e$ of the maximum value is the pulse decay time. Optical pulses from organic scintillators are often described by the full width of the pulse at the half maximum of intensity. Further details of the scintillation process can be found in the text by Knoll [1] and, in particular, the treatise by Birks [13].

Scintillator Types

As previously noted, the scintillation process is observed in solid, liquid, and gas phases, but gamma applications are limited mainly to solids and liquids. This brief discussion is confined to the most common solid and liquid phase scintillants that are applicable to gamma ray detection. A number of scintillators, including pure organic crystals and gas scintillators used primarily for charged particles, are not considered. Those remaining fall into inorganic and organic types.

Inorganics

The most important of this group are crystals of inorganic salts containing trace quantities of activators to enhance the emission. Because of their high atomic number, high density, and light output, they are valued for gamma spectroscopy. They are available commercially in a variety of standard forms, including right cylinders and parallelepipeds, and are readily machined to custom shapes. Ruggedness varies considerably among crystal types; care in packaging and use is required. Encapsulated crystals are available, but integrated units comprising a scintillator and photomultiplier are also available and often preferable.

The most widely used of this group is sodium iodide activated with thallium, NaI(Tl). NaI(Tl) has high light output and is generally the choice for scintillator-based spectroscopy systems. This material is hygroscopic and must be encapsulated. A typical pulse height spectrum from a NaI(Tl) photomultiplier combination is shown in [Figure 66.6](#).

Also useful for spectrographic applications is cesium iodide, which is available with either a thallium or sodium activator. The optical output of CsI(Tl) is at substantially longer wavelengths than either NaI(Tl) or CsI(Na) and is well matched to the spectral response of silicon. This has been successfully exploited to produce small, rugged CsI(Tl)-Silicon PIN devices. A spectrum of Cs-137 obtained with a CsI(Tl)/PIN detector combination is shown in [Figure 66.7](#). Exceptional resolution can be obtained when CsI(Tl) is used with a mercuric iodide photocell. With this combination resolution at 662 keV of better than 5 percent has been reported [14].

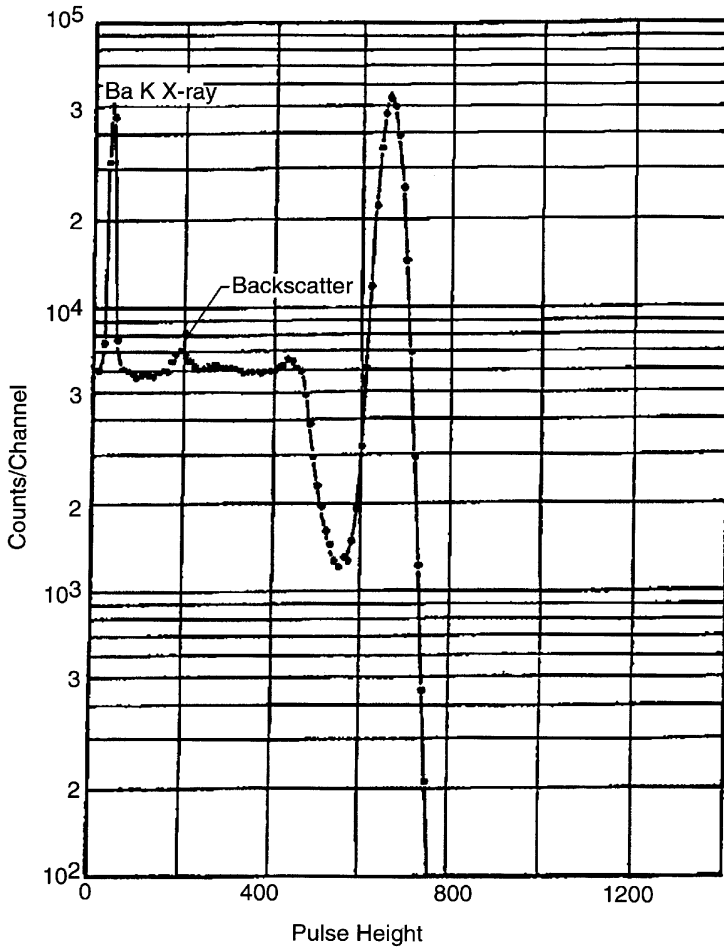


FIGURE 66.6 Typical energy spectrum obtained with a NaI(Tl) scintillator/photomultiplier combination in response to a Cs-137 source (662 keV).

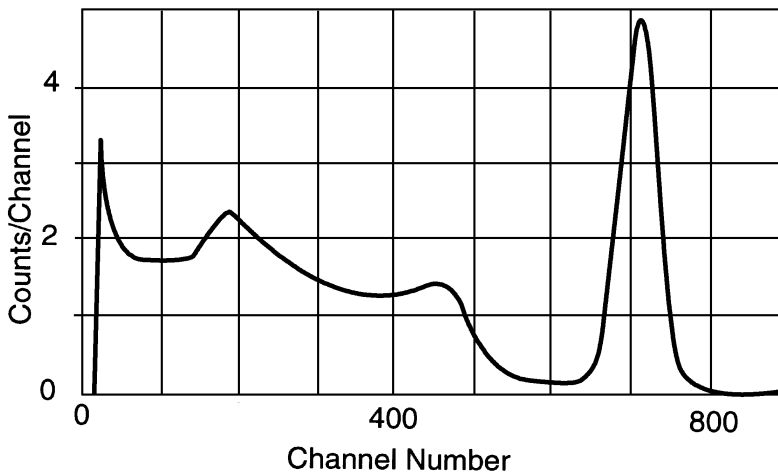


FIGURE 66.7 Energy spectrum of Cs-137 (662 keV) obtained with a CsI(Tl)/PIN combination. Specifications CsI(Tl): 1 cm \times 2 cm \times 2 cm; PIN: 1 cm \times 2 cm.

Two unactivated inorganic crystals, barium fluoride (BaF_2) and bismuth germinate ($\text{Bi}_4\text{Ge}_3\text{O}_{12}$), warrant comment. Barium fluoride has a weak subnanosecond component in the ultraviolet that is useful for timing and the recording of fast transients. With proper attention to ultraviolet transmission and photocell response requirements, gamma spectra can be obtained. Bismuth germanate has lower light output than either CsI or NaI and inferior energy resolution. However, because of its high density (7.1 g/cm^3) and the high atomic number (83) of bismuth, it is a good choice when high counting efficiency per unit volume rather than energy resolution is required.

Organics

Organic scintillators are available in both solid and liquid form. This group is characterized by very fast rise times (often subnanosecond) and decay times of a few nanoseconds. Their scintillation efficiency is about one-third that of the more efficient inorganics, however. Because of the low atomic number, photoelectric absorption is not significant. As a result gamma spectra consist mainly of a Compton continuum with, in large samples, a distinct Compton edge. Because of the absence of a photopeak, they are not well suited for spectroscopy applications. (High-Z additives such as tin or lead have been shown to enhance the photoelectric response but sometimes at the cost of light output.) They are particularly well suited for counting applications when very large detector volumes are required or for wide bandwidth measurements of fast transients. Because of the large number of available fluorescent organic compounds, organic scintillators are much more easily tailored to meet emission wavelength and decay time requirements than inorganics. The liquids typically consist of one or more fluorescent organic compounds dissolved in an aromatic solvent. A large number of formulations are commercially available. They can be obtained in sealed vessels suitable for mounting on a photomultiplier or as part of integrated scintillator–photomultiplier combination.

Solid organic solutions or plastic scintillator are prepared by dissolving fluorescent compounds in monomers of styrene or vinyl toluene, which then are polymerized. Like liquid organics, several different solutes can be used to achieve the desired wavelength and efficiency. Slabs of plastic scintillator several meters in length can be prepared in this manner. Alternatively, custom shapes can be either cast directly or machined.

Characteristics of several representative scintillators are shown in [Table 66.2](#).

TABLE 66.2 Properties of Common Scintillators

Scintillator	Wavelength of Emission Maximum (nm)	Density (g/cm^3)	Principle Decay Constant (ns)
NaI(Tl)	415	3.67	230.0
CsI(Tl)	530	4.51	1000.0
CsI(Na)	430	4.51	630.0
BaF_2	220	4.88	0.6
$\text{Bi}_4\text{Ge}_3\text{O}_{12}$	460	7.13	300.0
BC-505 (liquid)	425	0.88	2.5
BC-400 (plastic)	423	1.032	2.4

Source: Bicron, 12345 Kinsman Road, Newberry, OH 44065-9577.

66.2 Germanium Detectors

High-purity germanium (HPGe) detectors are widely used for gamma-ray spectroscopy due to their combination of efficient absorption and high energy resolution. [Figure 66.8](#) shows the cross sections of germanium and silicon for photoelectric absorption, Compton scattering, and absorption by electron-positron pair production in several materials used for solid-state nuclear radiation detectors. Attenuation is significantly stronger in germanium than in silicon. Over much of the gamma spectrum, the dominant

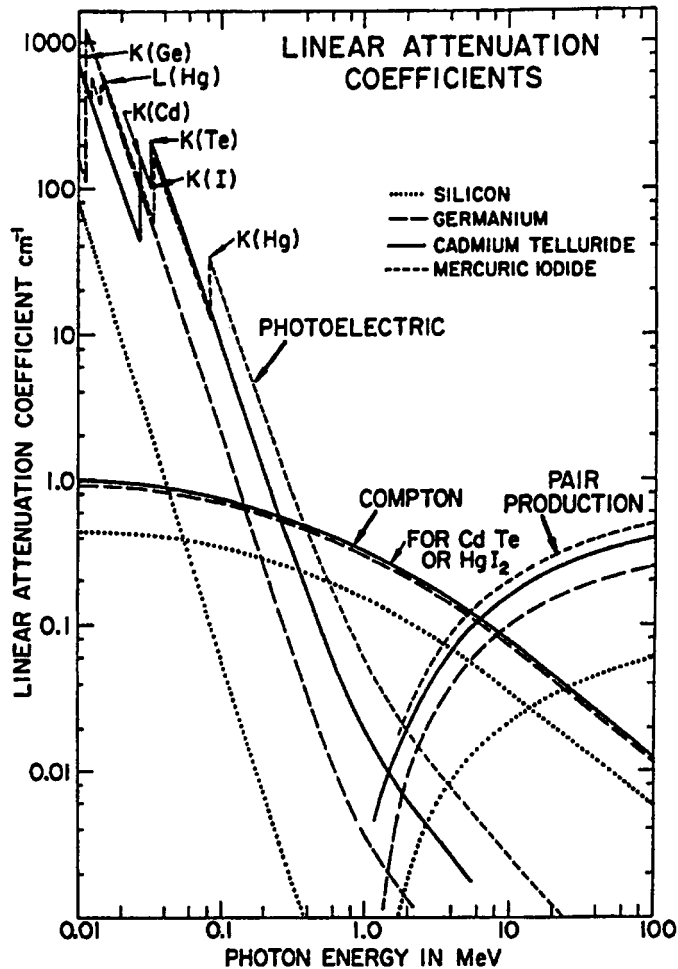


FIGURE 66.8 Attenuation coefficients vs. energy in common semiconductor materials [4].

interaction is Compton scattering. However, it is principally the stronger photoelectric absorption in germanium that makes it more suitable than silicon for gamma-ray spectroscopy. In the typical size germanium detector, a gamma ray may be scattered several times before it is photoelectrically absorbed. Thus, the energy of the gamma ray is primarily transmitted directly to a small number of electrons. These energetic electrons in turn interact with electrons in the valence bands to create mobile pairs of electrons and holes. In a detector with sufficiently large volume, the average number of electron-hole pairs N produced by an absorbed gamma-ray of energy E becomes independent of the details of the initial reaction path and varies linearly with E as follows:

$$N = \frac{E}{\epsilon} \quad (66.6)$$

This relationship is more broadly valid and is the foundation of energy spectroscopy of gamma rays using semiconductors, gases, and cryogenic liquids (ϵ depending on the material). While ϵ is independent of the gamma-ray energy (and is also virtually the same for energy deposited by charged particles), ϵ in germanium does increase slightly with decreasing temperature, as does the energy gap. At 77 K, ϵ is 2.96 eV, and the energy gap is 0.72 eV.

Practical exploitation of Equation 66.6 depends on electronically detecting the motion of the ionized charge in an electric field. The signal-to-noise ratio is improved by reducing current flow in the detector from other mechanisms. In germanium, this is achieved by producing a rectifying and a blocking contact and by cooling to about 100 K. For a planar detector, a slice of high-purity germanium is diffused with the donor lithium on one side, forming a strongly n -type layer. The opposite side is implanted with the acceptor boron, forming a p + layer. When voltage is properly applied, the electric field direction prevents the majority carriers in the contact regions from being injected across the device. As the voltage is applied, a region depleted of holes will advance into the slice from the n + contact if the slice is p -type. If the slice is n -type, a region depleted of electrons will advance from the p + contact. At the depletion voltage V_d , the depletion region reaches the opposite contact. For germanium,

$$V_d = 565 V \times \frac{N_e}{10^{10} \text{ cm}^{-3}} \times \frac{d^2}{\text{cm}^2} \quad (66.7)$$

N_e is the net charge density in the depleted or active region of the detector, and d is the thickness of this region. This is a key relationship in high-purity germanium technology, as it quantifies the effect of the residual impurity concentration on device size and depletion voltage. Techniques to grow germanium pure enough for gamma detectors were pioneered by Hall [15] and the detector group at Lawrence Berkeley Laboratory (Haller, Hansen, and Goulding [16]), based on purification methods of Pfann [17] and crystal-growing techniques developed by Teal and Little [18] to produce crystals for germanium transistors.

Leakage Current

Germanium detectors need to be cooled to reduce leakage current. There are several potential sources of leakage current, including

- Diffusion of minority carriers from either doped contact into the depletion region
- Thermal generation of carriers at either bulk or surface defects in the depletion region
- Electrical breakdown at points where the electric field is concentrated due to irregularities in the contact geometry, large-scale inhomogeneities in the bulk, or surface states.

Current will also be generated if the detector is not shielded from room-temperature infrared radiation. Background nuclear radiation from materials near the detector and cosmic radiation also generate leakage current.

Germanium detectors are typically liquid-nitrogen cooled and operated between 85 K and 100 K. In this temperature range, leakage current is typically less than 40 pA in “good” detectors and is not a significant contributor to system noise (400 to 900 eV). Leakage current increases with temperature and eventually becomes the predominate noise component. Pehl, Haller, and Cordi [19] reported a leakage current driven system noise of 2 keV at 150 K and 7 keV at 170 K for an 8 cm³ planar detector. These authors also reported that, above about 120 K, the leakage current had an activation energy of approximately one-half the bandgap and attributed this to generation at mid-gap surface states. Below 120 K, the temperature dependence was milder.

A typical detector/cryostat configuration is shown in [Figure 66.9](#). The detector resides in an evacuated cryostat and is cooled by means of a copper rod inserted into a liquid-nitrogen dewar. The first stage of amplification is an FET, also cooled, positioned nearby the detector. Mechanical fixturing is designed to stabilize the detector and the mechanisms for contacting it, to provide a cooling path from the detector to liquid nitrogen, and to electrically insulate the high-voltage contact.

A variety of detector geometries are shown in [Figure 66.10](#). These different electrode configurations allow efficiency and energy resolution to be optimized for different gamma-ray energies and applications. For example, the detector in [Figure 66.10\(c\)](#) minimizes noise by the lower capacitance of its electrode

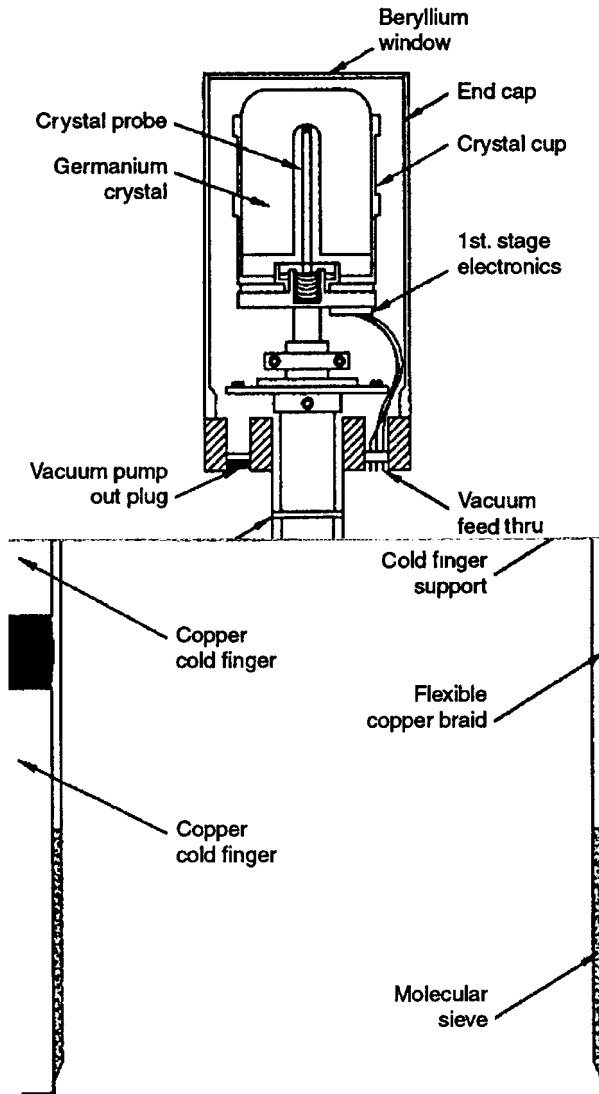


FIGURE 66.9 Schematic cross section of a dipstick cryostat. (Darken and Cost, 1993, reprinted with permission of Oxford Instruments, Inc.)

configuration at the expense of the reduced stopping power. Thus, this detector would be more suitable for lower-energy gamma rays.

Coaxial Detectors

The detector type shown in Figures 66.9 and 66.10(e) has a closed-end coaxial geometry. Nearly all of the largest-volume (active volumes of 100 cm³ to 800 cm³) HPGe detectors are of this type. This electrode geometry reduces both capacitance and depletion voltage with respect to a planar detector of the same volume. This latter benefit relaxes the constraint on material purity. In addition, charge collection distances are shortened, and the uncontacted surface area, frequently troublesome in processing, is reduced. Also, the HPGe is grown by the Czochralski technique and is therefore nearly cylindrical, even before machining. It is important, however, to note that the reduction in depletion voltage is realized only when the device is contacted so that it depletes from the outer contact to the inner contact. Thus,

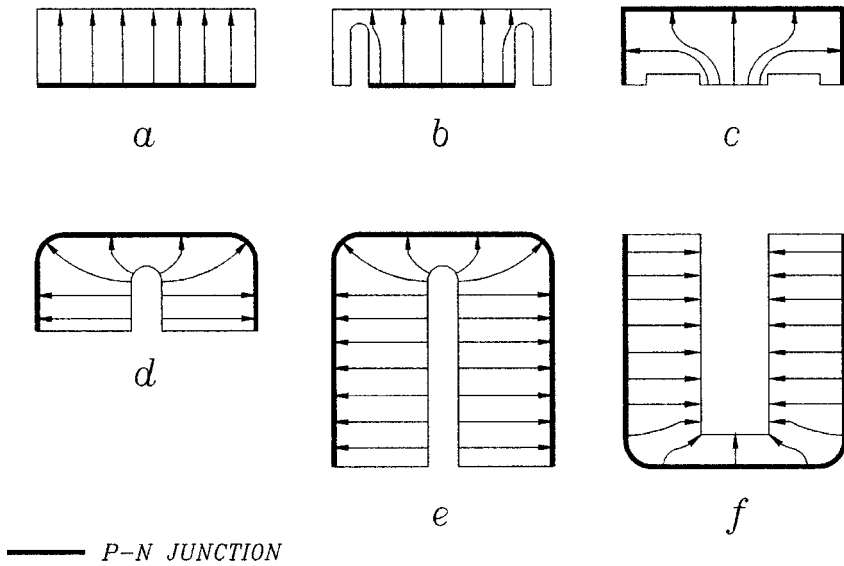


FIGURE 66.10 Schematic cross section and electrostatic field distribution in high-purity germanium detectors. The dark line represents the p - n junction: (a) true planar, (b) grooved planar, (c) low capacity planar, (d) truncated coaxial, (e) closed-end coaxial, and (f) well geometry.

p -type HPGe to be fabricated into a coaxial detector is lithium diffused on the outer diameter and, in the case of n -type HPGe, the outer diameter is boron implanted.

The boron-implanted contact (depth approximately $0.2 \mu\text{m}$) is thinner than the lithium-diffused contact (depth approximately $750 \mu\text{m}$), so the n -type coaxial detector can detect lower-energy radiation and is usually built with a beryllium window in the aluminum end cap to take full advantage of this feature. The difference in the range of use is illustrated in Figure 66.11. The geometric asymmetry of the

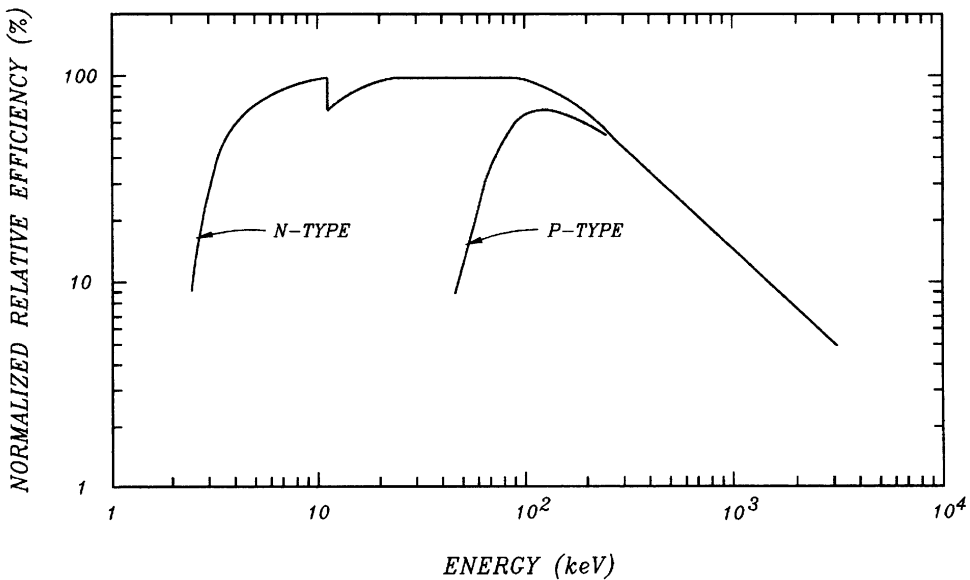


FIGURE 66.11 Relative absorption efficiencies for typical n - and p -type detectors. (Darken and Cox, 1993, reprinted with permission of Oxford Instruments, Inc.)

contacting electrodes in the coaxial detector makes charge collection more dependent on the carriers (electrons or holes) traversing to the inner contact. As more gamma rays are absorbed near the outer contact, the carriers traversing to the inner contact must travel on average a longer distance. Also, charge traversal near the inner contact is particularly effective in inducing current in the external circuit [20]. Thus, the *p*-type coaxial detector with positive bias on the outer electrode is more sensitive to hole collection, and the *n*-type coaxial detector with negative bias on the outer electrode is more sensitive to electron collection. This is a crucial consideration in applications where the hole collection is going to be degraded during use by exposure to fast neutrons or other damaging radiation. The superior neutron damage resistance of the electrode biasing polarity on *n*-type coaxial detectors was demonstrated by Pehl et al [21].

A typical gamma-ray spectrum of a Co^{60} source taken with a coaxial HPGe detector is shown in Figure 66.12. The salient features are the full-energy peaks at 1.17 MeV and at 1.33 MeV, and the lower energy plateaus due to incomplete energy absorption of Compton-scattered gamma rays. The peak-to-Compton ratio [22] is generally 40 to 100, depending on the size and quality of the detector. The 1.33 MeV peak is shown separately in Figure 66.13. The energy resolution measured as the full width at half the peak maximum (FWHM) for typical coaxial germanium detectors is between 1.6 and 2.1 keV for 1.33 MeV gamma rays, again depending on the size and quality of the detector. The variance in the peak L^2 (FWHM = $2.35 \times L$, L being the standard deviation for a Gaussian distribution) can be divided into three additive components: the electronic noise component L_N^2 , a component reflecting the variance in the number of electron-hole pairs created L_F^2 , and a component due to incomplete charge collection L_T^2 ,

$$L^2 = L_N^2 + L_F^2 + L_T^2 \quad (66.8)$$

$$L_F^2 = \epsilon EF \quad (66.9)$$

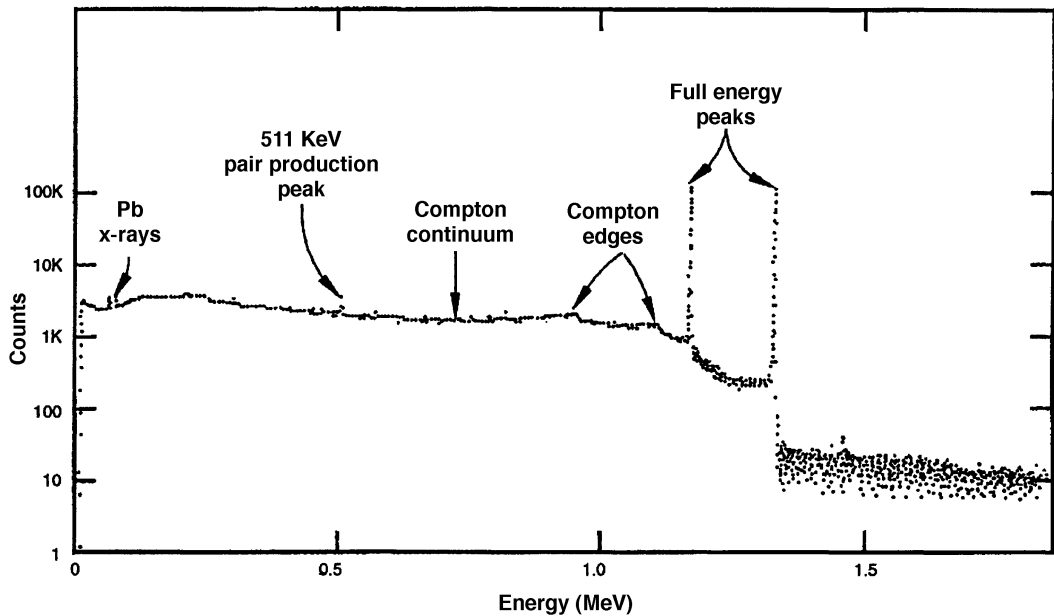


FIGURE 66.12 A Co^{60} spectrum collected with a 15% *p*-type detector showing typical features of germanium detector spectrum.

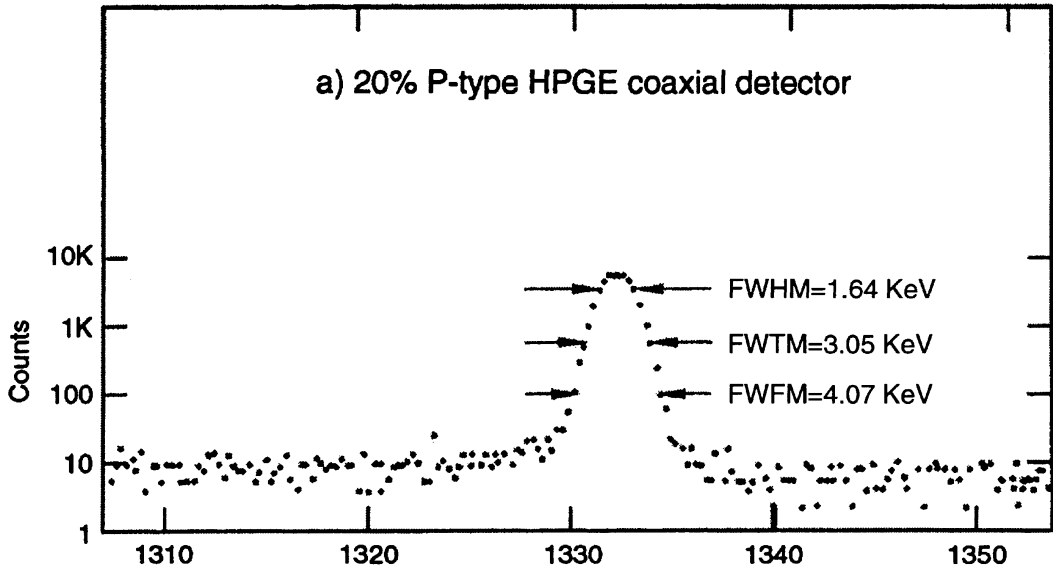


FIGURE 66.13 A ^{60}Co spectrum collected with a 22% relative efficiency *p*-type detector. (Darken and Cox, 1993, reprinted with permission of Oxford Instruments, Inc.)

F is called the Fano factor and has been experimentally determined to be no greater than 0.08 for germanium [23]. $F < 1$ implies that electron-hole pair creation events are not uncorrelated. L_T^2 is usually dominated by the trapping of electrons and holes at defect sites. However, shorter electronic shaping times, lower electric fields, and larger detectors accentuate ballistic deficit (loss of collected charge in the external electronics due to the finite traversal time of the electrons and holes across the detector). L_N^2 is independent of gamma ray E and is the dominant resolution limiting factor at low energies. L_F^2 depends linearly on E and, for a coaxial detector, usually dominates L_N^2 for E over a few hundred keV. The energy dependence of L_T^2 is not given simply from first principles for an arbitrary trap distribution, but an E^2 dependence seems to fit under many circumstances. Thus, at high enough E , L_T^2 is expected to be the largest component. For “good” detectors at 1.33 MeV, however, L_T^2 is always smaller than L_F^2 . In addition, the magnitude of L_T^2 is variable enough between detectors that it distinguishes between acceptable, very good, and excellent detectors. L_T^2 is usually also the only component of resolution drawn from a nongaussian distribution and is thus responsible for any low-energy tailing of the peak.

X-Ray Detection

Both silicon and germanium detectors are used in low noise systems for the detection of fluorescent X-rays produced by electron beams (usually in an electron microscope) or X-rays (XRF). For both materials the detector is liquid-nitrogen cooled to reduce leakage current, and small volume devices [Figure 66.10(b), typically 10 mm² active area, and 3 mm depth] are used to decrease capacitance and therefore to further reduce electronic noise. Lithium-drifted silicon (SiLi) detectors were used first for these applications. Early germanium detectors displayed poor peak shape for X-ray energies just above the L absorption edges (attributed to diffusion against the field to the front contact by some electrons and their resulting loss to the photopeak [24]). However, as was first demonstrated by Cox et al., [25] this is not a fundamental problem but can be solved by the contacting technology. An X-ray spectrum taken with a HPGe detector is shown in Figure 66.14. Germanium has the advantages with respect to silicon of a smaller ϵ (2.96 eV per pair versus 3.96 eV per pair at 77 K) for better energy resolution and a higher Z (32 versus 14) for better photoelectric absorption of higher-energy X-rays.

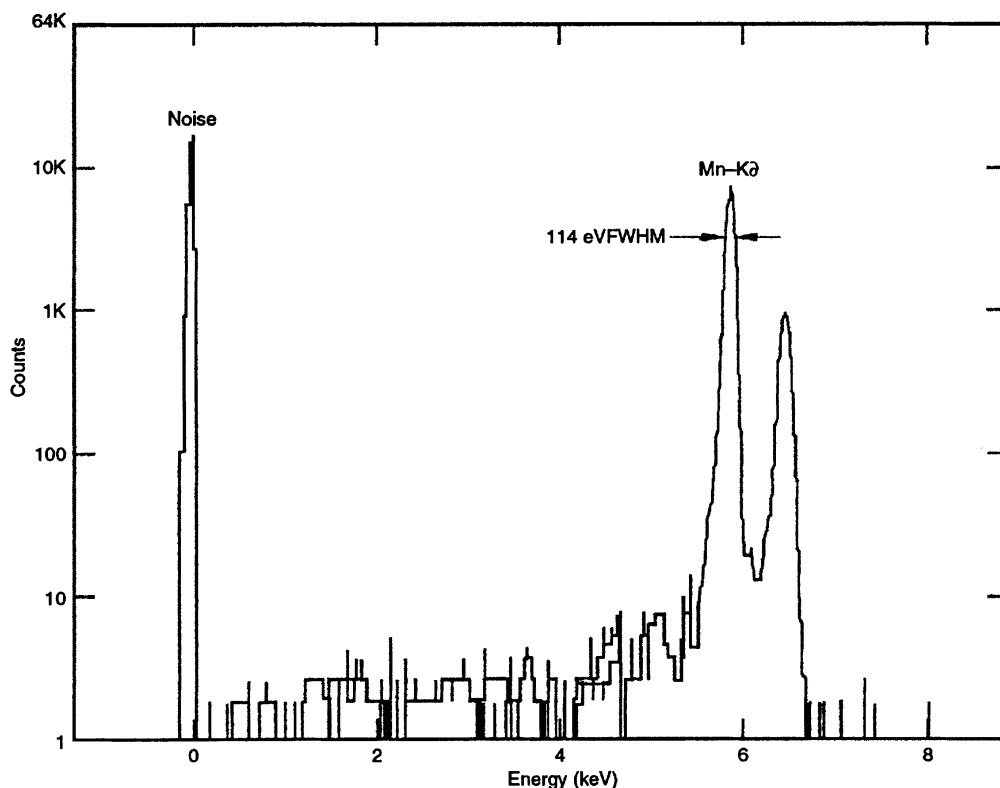


FIGURE 66.14 Manganese X-ray spectrum from ^{55}Fe source collected with an HPGe detector. (Darken and Cox, 1993, reprinted with permission of Oxford Instruments, Inc.)

Current Status of HPGe Detector Technology

High-purity germanium detectors are a mature commercial technology. Process development in crystal growing and diode fabrication have been conducted in private industry where significant advances are proprietary. However, the results of technological advances in these areas are quite evident in the continual improvement in the size, performance, and availability of HPGe detectors. Maximum photopeak efficiency for HPGe gamma-ray detectors is doubling every 6 to 8 years. Concurrently, energy resolutions are moving toward the theoretical limits of Equation 66.8 as the concentrations of trapping centers are reduced.

The reliability as well as the performance of germanium gamma-ray detectors has also continued to improve, although this is harder to quantify. Cryostats have been redesigned to reduce virtual and direct leaks, reduce microphonics, implement modular design, and to improve ruggedness. Detector makers are also making more serious attempts to offer models with reduced backgrounds by judicious design changes and careful selection of materials.

New applications for gamma-ray spectroscopy have emerged. The HPGe detector industry has recently supplied over 100 detectors each to two different experimental facilities (GAMMASPHERE in the United States, and EUROBALL in Europe), where they were arranged spherically in a modular fashion around the target of an ion accelerator to study the decay of nuclei from excited states of high angular momentum.

For users of single-detector systems, developments in the pulse processing electronics necessary for data acquisition and in the hardware and software for data analysis have resulted in both more compact and more flexible systems. Plug-in cards for a personal computer are available that not only contain the functions of the ADC and multichannel analyzer, but the high-voltage power supply and amplifier as well. Software developments also allow for control of many pulse-processing parameters that were previously set manually.

66.3 Silicon Detectors

As with germanium for gamma-ray spectroscopy, the impurity requirements on silicon for nuclear radiation detectors are also stringently low—and difficult to obtain. Such silicon must be grown by the float zone technique to eliminate contamination from a crucible. Unlike with germanium, little dedicated effort has been expended trying to improve silicon growth techniques to achieve superior detector characteristics. Most progress in material quality has come from technology improvements aimed at other applications. The purest silicon commercially available typically has a net electrically active impurity concentration of a few times 10^{11} cm^{-3} (compared to 10^{10} cm^{-3} for HPGe), which usually limits device thicknesses to less than 1 mm. However, this thickness is sufficient for many applications. Silicon detectors are widely used for heavy charged particle (alpha, proton, ion) spectroscopy. When thicker silicon devices are required (X-ray spectroscopy, beta spectroscopy, or medium-energy protons: $E > 25 \text{ MeV}$), silicon of higher net purity may be obtained by lithium drifting [26], but such material cannot be subsequently processed above room temperature.

In contrast to germanium detectors, silicon detectors can be operated at room temperature. Compared to gas and scintillation detectors, silicon detectors have good energy resolution and are reasonably compact. They are fabricated from slices of a silicon single crystal and are available in a variety of areas (25 to 3000 mm^2), and the active thickness is usually a few hundred micrometers. Specialized detectors have been developed for a wide variety of applications.

Energetic heavy charged particles lose kinetic energy continuously along a linear path in an absorbing material. Energy is transferred primarily to the electrons in the absorbing material but to a lesser extent to the nuclei also, via Rutherford scattering. Although only energy transferred directly to the electronic system generates electron hole pairs, Equation 66.6 (with $\epsilon = 3.62/\text{pair}$ for silicon at 300 K) is still a good approximation. Energy loss is characterized by two parameters: specific ionization loss dE/dx , which depends on the incident particle, its energy, and the absorbing material, and the range R (i.e., the penetration depth of the particle), which determines the detector thickness required for complete energy absorption. The continuous nature of energy loss leads to substantial window effects.

Diffused Junction Detector

Silicon detectors can be generically categorized by the type of rectifying contact employed. The diffused junction detector is fabricated by diffusing phosphorus from the gas phase into p -type silicon. This is a high-temperature (900 to 1200° C) operation that is prone to introducing faster diffusing metals into the bulk that can act either as generation centers increasing leakage current, or as trapping centers degrading charge collection. The thickness of the diffused region, from 0.1 to 2.0 μm , also presents a dead layer to incident particles that is reduced in alternative technologies. Nonetheless, these detectors find use due to their ruggedness and economy.

Surface Barrier Detector

Surface barrier junctions are fabricated by either evaporating gold onto n -type silicon or aluminum onto p -type silicon. A typical entrance window is equivalent to 80 nm of silicon. The rectification properties depend on the charge density of surface states of the silicon and of the thin oxide layer over the silicon, as well as on the evaporated metal. The wafer is epoxied in an insulating ring before metallization. The finished detector is encapsulated in a can that has a front window for particle entry and a single contact in the back for the combined function of applying bias and for extracting the signal pulse. Devices can be operated either in the partially depleted or totally depleted mode. As fabrication is entirely at room temperature, there is no opportunity for metal contamination by diffusion. Generally, surface barrier detectors have lower leakage current, and less system noise than a diffused junction detector of comparable area and depth. However, detectors currently fabricated by ion implantation have still lower leakage current and electronic noise, together with a thinner and more rugged front contact. On the other hand, implanted detectors are not available in the same range of active thicknesses as surface barrier detectors. Below 100 μm and above 500 μm , only surface barrier

detectors are currently available. Surface barrier detectors can be made in small quantities with rather simple equipment.

Ion Implanted Detectors

A simplified representation of ion implanted detector fabrication is shown in Figure 66.15. The first successful implementation of silicon planar processing to silicon detectors was reported by Kemmer [27]. The procedure starts with the thermal growth of an oxide film on a high-purity, *n*-type silicon wafer. Windows are then opened in the oxide by photolithographic techniques. The front contact area is implanted with boron to form the rectifying contact, and arsenic is implanted into the backside. The wafer is then annealed to activate the implant, and aluminum is evaporated on both sides to reduce sheet resistivity. Typical entrance windows are 50 nm silicon equivalent. Electrical connections are made by wire bonding to the aluminum layers. Finished detectors are canned in a manner similar to surface barrier detectors. More than one detector can be fabricated on the same wafer using the appropriate masks during photolithography. In fact, quite elaborate detector geometries can be achieved via photolithography. The detector in Figure 66.15 is actually a strip type.

This ion implantation planar process technology is well suited for mass production of wafer sizes compatible with the rest of the silicon industry. Minimum wafer diameters are now 4 or 5 in. At this diameter, breakage during fabrication is an issue for thicknesses less than 150 μm. For thicknesses greater than 500 μm, the availability of enough sufficiently pure material to justify the cost of photolithographic masks is an issue. Ion implanted detectors can be baked at 200° C to reduce outgassing. This is a significant improvement over surface barrier detectors, which irreversibly degrade by device processing above room temperature. This is a useful feature, as most heavy charged particle spectroscopy is done in a vacuum.

Leakage currents, at room temperature, are typically 1 to 10 nA per cm² active area and per 100 μm depletion depth. These values represent an order of magnitude reduction in leakage current with respect to surface barrier detectors. Two factors are relevant. Passivation of silicon surfaces by thermal oxidation

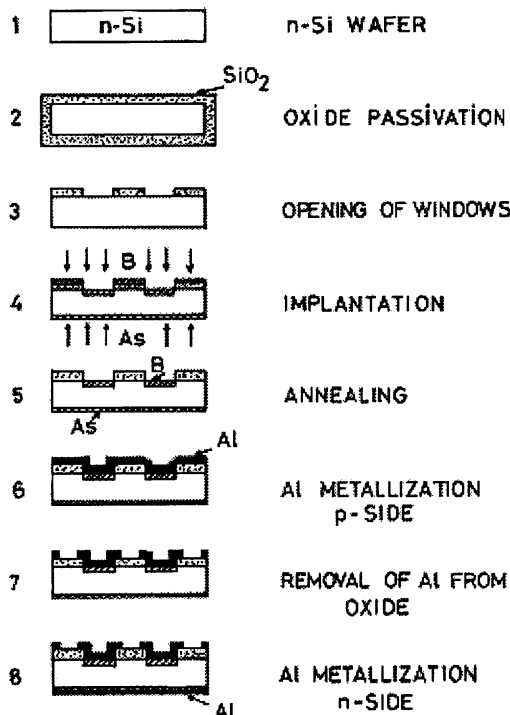


FIGURE 66.15 Steps in the fabrication of passivated planar silicon diode detectors. (From Ref. 30.)

is extremely effective in reducing leakage current around the rectifying contact. Also, the bulk generation current is reduced by the gettering of metal impurities during the high-temperature oxidation. Float zone silicon for radiation detectors usually has a minority carrier lifetime longer than 1 ms and this can be increased an order of magnitude during detector fabrication [28]. Thus, not only is leakage current reduced, but potential charge collection problems are also eliminated.

Energy Resolution

A typical spectrum of an Am-241 alpha particle source taken with an ion implanted detector is shown in Figure 66.16. While the factors considered in Equation 66.8 for germanium gamma-ray spectrometers are still valid, additional considerations also apply. In particular, if the source is moved closer to the detector to improve collection efficiency, larger differences in the angle of incidence will produce peak broadening due to larger variation in effective window thickness. Even when the source is sufficiently distanced from the detector, there will still be spatial variations in window thickness, as well as some variation in energy lost escaping from the source and traversing to the detector.

Another source of peak broadening is the variation in the small amount of particle energy lost during Rutherford scattering. This energy is transmitted directly to the scattering nuclei and does not generate electron-hole pairs, and a small pulse deficit results. These events are relatively few but large and therefore contribute disproportionately to peak variance. The FWHM contribution of this effect on a 6-MeV alpha particle peak has been estimated to be 3.5 keV [29].

Spatial Resolution

The uninterrupted progress of the semiconductor silicon industry in achieving both larger wafers and smaller device features has allowed the development of larger and more complex silicon detectors that can provide position information in addition to (or instead of) energy information. Spatial detection can be obtained by fabricating detectors as pixels (two-dimensional) or strips (one-dimensional) on the same wafer. For penetrating radiation, two strip detectors, one behind the other but with the strip pattern rotated 90°, provide two-dimensional positioning. Frequently, such detectors are individually designed and fabricated for a particular application. Strip detectors, drift detectors, and CCD (charge-coupled device) detectors will be discussed here.

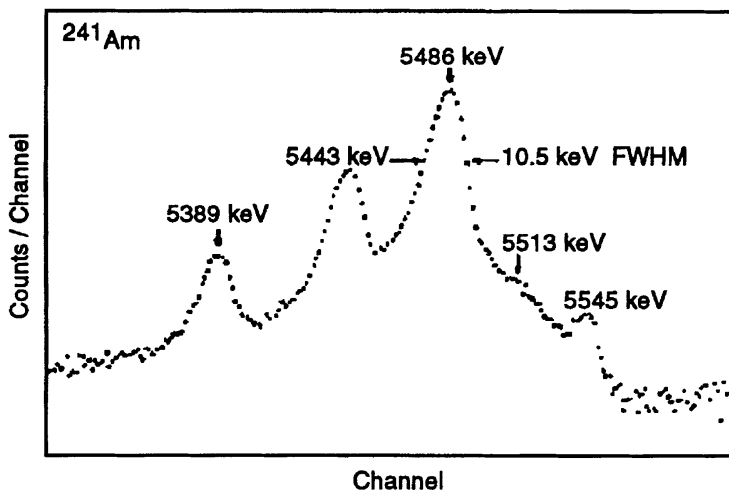


FIGURE 66.16 Spectrum of a ²⁴¹Am alpha-particle source (log scale) measured with an IP detector (25 mm² area, 300 μm thick) at room temperature. Resolution at 5.486 MeV is 10.6 keV (FWHM). (From Ref. 30).

Strip Detectors

Silicon strip detectors are currently fabricated on silicon wafers (typically approximately 300 μm thick) by using photolithographic masking to implant the rectifying contact in strips [30]. The strips usually have a pitch on the order of 100 μm and a width less than half of this size to minimize strip-to-strip capacitance and hence electronic noise [31]. The device is biased past depletion, and the back blocking contact is continuous. Each strip requires, in principle, its own signal processing electronics; however, charge division readout (capacitive or resistive) can reduce the number of amplifiers by a factor of 10. Detectors are fabricated in rectangular segments from a single wafer and can be ganged together if a larger area is needed.

Strip detectors are well established in high-energy physics experiments for reconstruction on the micron scale of the tracks of ionizing particles. The particles being tracked result from the collision of accelerated particles with a target and are highly energetic ($>10^{10}$ eV). Frequently, experimental interest is focused on short-lived particles created in the collision but which decay before they can be directly detected. Spatial resolution of the decay vertex from the original collision is necessary to detect such a particle and to determine its lifetime.

The requirements of new high-energy experiments and advances in silicon technology have produced much evolution and innovation in the strip detector concept. For example, a double-sided microstrip detector with an oxide-nitride-oxide capacitor dielectric film has been reported [32]. The use of intermediate strips to improve spatial resolution has become common [33], and the biasing network has been integrated onto the detector [34].

Drift Detectors

Silicon drift detectors were first proposed by Gatti and Rehak [35] as an alternative to silicon strip detectors in high-energy physics experiments. The primary motivation was to significantly reduce the number of readout channels. Drift detectors have subsequently been adapted for X-ray spectroscopy. These detectors are usually fabricated on n -type silicon wafers with holes collected to either a p^+ contact on the back side of the detector, or to concentric annular p^+ contacts on the front side. The detector is depleted from both sides. The reverse bias applied to the p^+ annular rings is varied in such a way that electrons are collected radially in a potential energy trough to an n^+ anode at the center of the detector on the front side.

A cross section through a circular drift detector is shown in Figure 66.17. The electron collecting anode ring surrounds the integrated FET used for the first stage of signal amplification. Enough negative bias

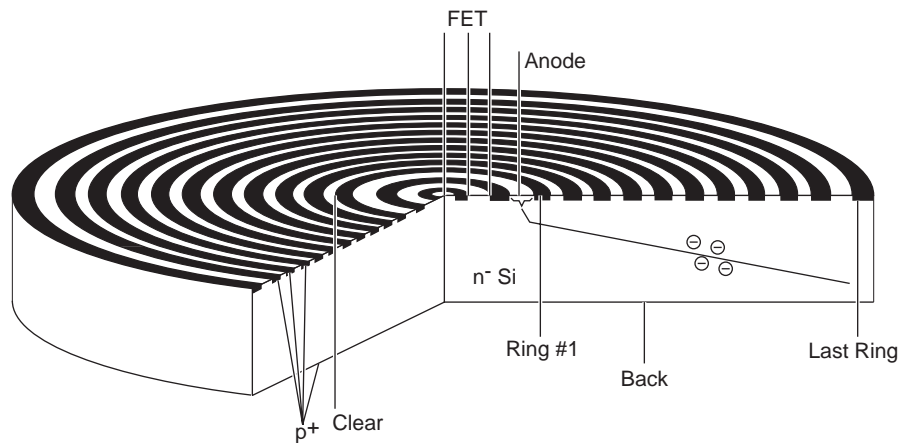


FIGURE 66.17 Cross section of a cylindrical silicon drift detector with integrated n -channel JFET. The gate of the transistor is connected to the collecting mode. The radiation entrance window for the ionizing radiation is the non-structured backside of the device.

is applied to the back contact (actually the entrance window) to deplete the wafer to the anode, which is near ground potential. At the same time, negative bias, progressively increasing in magnitude, is applied from the ring next to the anode (near ground potential) to the outermost ring, which is maintained at about two times the bias of the back contact. These applied biases deplete the detector in such a way that there is an electrostatic potential minimum for electrons that varies in depth across the detector from right under the front surface at the anode to near the back contact at the last ring. Ionized electrons will drift first to this minimum, then drift radially to the anode as shown in Figure 66.17. A feature of this contacting arrangement is that the anode capacitance, and hence amplifier series noise is low and nearly independent of the active area of the detector.

Silicon drift detectors have been designed in several different topologies of various sizes for different experimental needs. Spatial resolution for tracking and vertexing of high-energy particles is obtained by segmenting the cathode (for angular position) and analysis of signal rise time (for radial position [36]). Drift detectors with integrated electronics have been demonstrated for high-resolution room-temperature X-ray spectroscopy [37].

CCD Detectors

The design of CCD (charge coupled device) detectors has similarities to the silicon drift detector [35]. The CCD detector is normally fabricated on an *n*-type silicon wafer depleted both from the backside with a continuous *p*+ contact on the back, and from *p*+ CCD registers on the front. Reverse bias voltages are such that the wafer is totally depleted and the electron potential minimum is about 10 μm below the CCD registers. After an ionizing event, holes are collected to the *p*+ contacts, and electrons are trapped under a nearby register, then transported down a channel of registers by properly clocked voltage pulses to the registers. Each channel has its own readout anode, which can be made small to minimize capacitance, a prerequisite for minimizing noise. The first stage of amplification is frequently integrated onto the same wafer. Spatial resolution is limited to the register (pixel) size. Brauniger et al. [38] described initial results on a 6×6 cm CCD array of 150×150 μm pixels intended for satellite X-ray imaging. The system also had an energy resolution of 200 eV FWHM for 5.9 keV X-rays at room temperature.

Silicon pixel detectors have also been designed using other highly integrated device structures to optimize particular performance aspects such as timing resolution. Pixel detectors using MOS transistors [39] and using reverse-biased diodes with individual readout circuitry [40] have been described.

Present Status of Silicon Detector Technology

The simple structured silicon detectors fabricated with parallel contacts on a silicon wafer continue to serve a well established need for charged particle spectroscopy. Where economies of scale can be applied, ion implanted detectors have replaced surface barrier detectors. In X-ray spectroscopy for microanalysis (SEM and XRF), liquid-nitrogen-cooled Si:Li detectors are being challenged by similarly sized HPGe detectors, but Si:Li are still more widely used. In projects of sufficient size to support their development, specialized low-noise silicon drift detectors and CCD-based detectors have been designed and fabricated with promising room-temperature energy resolution: 200 eV FWHM at 5.9 keV. These highly structured detector technologies may find future application in liquid-nitrogen-cooled or room-temperature systems for microanalysis using X-ray spectroscopy.

In high-energy physics, the use of various strip, drift, and pixellated detectors for tracking and vertex determination has flourished. These efforts will intensify as experimental requirements for spatial resolution increase. However, radiation damage to the detector is already an issue in this application, and higher luminosity beams will only increase the problems. Nevertheless, it appears that the continuing need of the high-energy physics community for a higher number and density of signal paths forecasts continued reliance on the ever-improving integration technology of the semiconductor silicon industry.

66.4 Room-Temperature Semiconductors

Applications arise that require energy resolution beyond the capability of scintillator systems and where cryogenically cooled semiconductors are not suited. Examples include detector probes for monitoring restricted areas, monitoring at remote sites where replenishing the coolant is impractical, spectral imaging, and many portable instrument applications. There is available a class of semiconductor detectors that satisfy many such needs by providing energy resolution substantially better than the best scintillators (although inferior to cooled semiconductors) while operating at ambient temperature. In addition to spectroscopy, these devices are also useful for counting applications where high detection efficiency per unit volume is required. In these applications, the devices are operated in pulse mode wherein the charge associated with single-photon absorption events is recorded. They also can be operated in a current mode in the manner of a solid-state ion chamber. In their current stage of development, room-temperature detectors are limited in size and best suited for the energy region below 1 MeV.

The room-temperature detectors are distinguished from cryogenic semiconductors by the magnitude of the energy gap that separates the normally vacant conduction band from the highest filled band. If this energy gap is small, as is in the case of silicon (1.14 eV) and germanium (0.67 eV), electrons can be thermally stimulated across the bandgap at room temperature. The resultant current competes with the gamma-ray-generated signal precluding room-temperature operation of germanium and high-resolution applications of silicon. Thermally stimulated current is reduced to acceptable levels at bandgaps energies of about 1.4 eV and above. This phenomenon has been successfully exploited in the development of room-temperature detector materials including cadmium zinc telluride (acronym, CZT), cadmium telluride (CdTe), and mercuric iodide (HgI₂).

Theory of Operation

Operating principles of room-temperature detectors are similar to those governing the more familiar cryogenic semiconductor devices. Gamma radiation is absorbed in the material and generates electron-hole pairs that move under the influence of an applied electric field to contacts and external electronics for processing and production of the familiar pulse-height spectrum. The process is shown schematically in Figure 66.18. Fundamental to the charge transfer process is the carrier mobility (μ) and the carrier life time (τ). The product $\mu\tau E$ defines a drift length (λ) that should be long compared to the intercontact dimensions. Owing to the substantially higher average atomic number of the room-temperature detector materials in the gamma absorption cross sections, the probability of gamma ray absorption is much

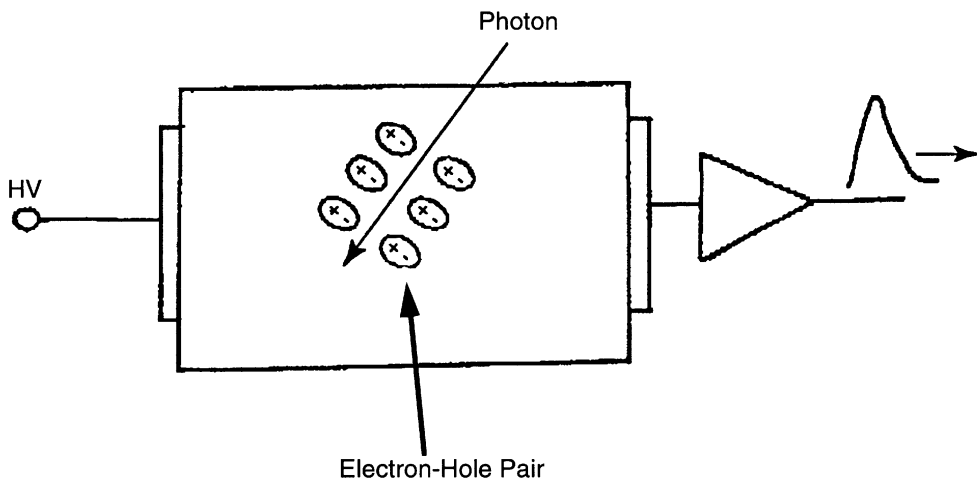


FIGURE 66.18 Schematic illustration of charge generation in a planar detector.

higher than in silicon or germanium (Figure 66.8). As a result, room-temperature detectors provide greater detection efficiency per unit thickness.

The energy required to produce an electron-hole pair (ϵ) is typically a few times the energy bandgap of the material. In silicon where the bandgap is 1.14 eV, the energy to produce an electron-hole pair (ϵ) is about 3.5 eV. The absorption of a 1 MeV photon in silicon thus produces about 285,000 pairs. Values of ϵ for room-temperature materials are in the region 4.2 to 5.0 eV per e-h pair (see Table 66.3) and, consequently, fewer electron-hole pairs are generated per unit of absorbed energy. Complete collection of the charge is desired, although charge trapping, which may not affect the two carrier types equally, prevents this in most cases. The drift length for holes (λ_h) in these materials is often less than the intercontact dimensions and creates a condition where the collection efficiency depends on the photon interaction depth. This is phenomenon is illustrated in Figure 66.19, where induced charge from single gamma absorption events originating at various depths in the material is plotted as a function of time. The initial fast-rising segment is due to the more mobile electrons; the slower component is due to holes. In this example, hole trapping is assumed and is manifest in the curvature of the hole segment. The charge collection efficiency (η) can be derived from the Hecht relation [41]. For a photon absorbed at a distance x from the cathode of a planar detector of thickness L operated with a uniform electric, the relationship becomes

$$\eta = \frac{\lambda_e}{L} \left[1 - \exp\left(-\frac{L-x}{\lambda_e}\right) \right] + \frac{\lambda_h}{L} \left[1 - \exp\left(-\frac{x}{\lambda_h}\right) \right] \quad (66.10)$$

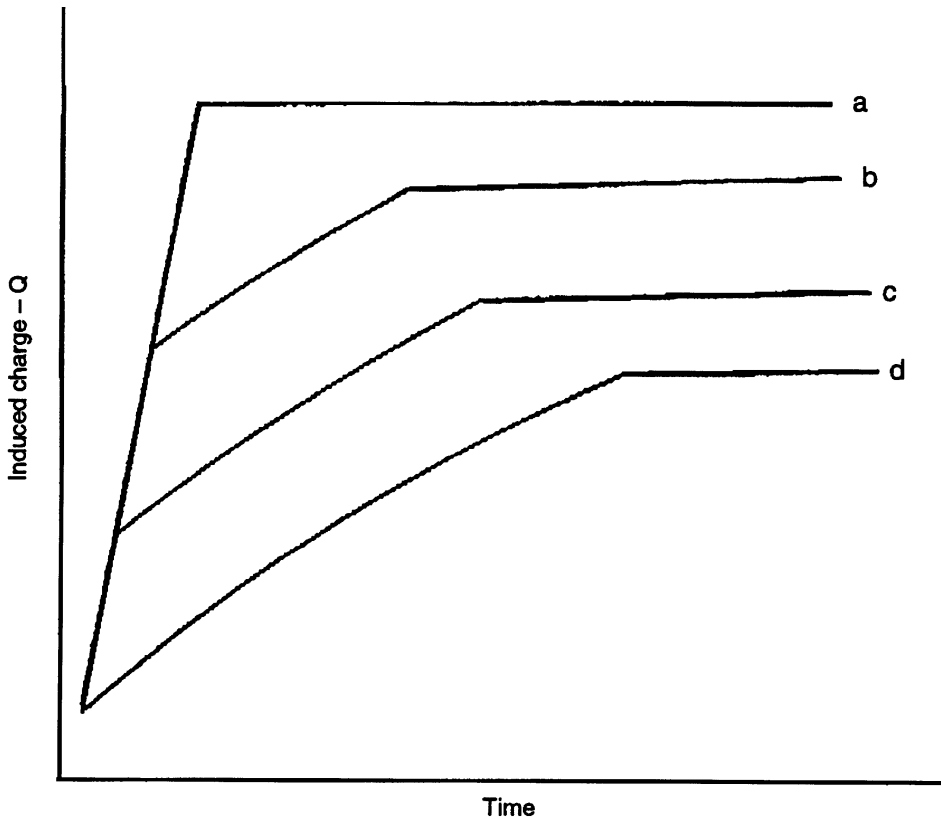


FIGURE 66.19 Charge collection in planar detector for single-photon interaction in a planar detector. Curves a through d depict the charge from photon interactions at increasing depths below the cathode.

TABLE 66.3 Physical Parameters of Common Room-Temperature Semiconductor Materials

Material	E_g (eV)	Z	ϵ (eV)	ρ (Ω)	$(\mu\tau)_e$ (cm^2/V)	$(\mu\tau)_h$ (cm^2/V)
Cadmium zinc telluride	1.65	48	5.0	10^{11}	1×10^{-3}	6×10^{-6}
Cadmium telluride	1.5	50	4.4	10^9	3.5×10^{-3}	2.3×10^{-4}
Mercuric iodide	2.13	62	4.2	10^{13}	1×10^{-4}	4×10^{-5}

Note: E_g = bandgap energy, Z = average atomic number, ϵ = energy to create an electron-hole pair, and ρ = resistivity.

Source: *Semiconductors for Room-Temperature Radiation Detector Applications*, R.B. James, T.E. Schlesinger, P. Siffert, and L.A. Franks (eds.), Materials Research Society, Vol. 32, Pittsburgh, PA, 1993.

The dependence of the collection efficiency on interaction depth reduces energy resolution and without mitigation would limit high resolution to thin devices. Fortunately, methods have been developed that permit high-energy resolution to be achieved in relatively thick samples. As with cooled semiconductor detectors, the energy resolution of the combined detector-electronics system is normally specified by the full width of a monoenergetic spectral peak at its half amplitude points (ΔE). The FWHM is in turn related to the variance in the peak L^2 (see Equation 66.8). It is useful to note that the energy resolution is related to the reciprocal of the product $\mu\tau$.

Operational Considerations

Important physical parameters for the leading room-temperature detectors are summarized in [Table 66.3](#). Detectors are available with surface area of a few square centimeters and thicknesses up to about 1 cm. The performance of detectors based on the different materials varies considerably, as can the performance for detectors of the same material. The choice of specific detector material is normally dictated by the application. The exceptionally high resistivity and high photoelectric cross section in mercuric iodide permit good resolution and high efficiency in the X-ray region, particularly below 10 keV. For example, ΔE of 4 percent has been reported [42] with typical values in the region of 10 percent. For applications in the region of 0.5 MeV, trade-offs between efficient gamma absorption and resolution may be required. If energy resolution is the primary concern, thinner devices that minimize charge trapping are generally required. Considerable progress is being made in achieving both high efficiency and resolution in the region of 0.5 MeV, particularly with CZT. For example, resolution of better than 3 percent has been achieved in 1-cm thick detector at 511 keV, and about 5 percent at 662 keV in a 2.5 cm thick device [4]. Improvements in material quality can be expected further improve the performance of thick detectors, as the $\mu\tau$ values are further increased.

Procedures have been developed to overcome many of the thickness and surface area limitations of currently available devices. For instance, electronic circuits have been developed that permit the operation of planar arrays that provide spectral resolution approaching that of single units while providing substantially greater area [43]. Similarly, high gamma absorption efficiency with useful spectral resolution has been obtained with stacks of thin spectrometer-quality detectors [44]. Additionally, pulse processing and single charge collection procedures have been demonstrated that enhance spectrometer performance. This development can be expected to substantially improve the availability and price of spectrometer grade devices. Further details concerning the performance of these devices, as well as electronic processing and design details, are available in the literature [2, 3, 45, 46].

Detectors based on the materials in Table 66.3 are available commercially. Due to the evolving nature of this technology, it is recommended that buyers' guides be consulted for suppliers and current availability.

66.5 Prices and Availability

The detectors described in this chapter are available commercially. Their prices vary widely, depending on type, size, and performance. Gaseous detectors are normally in the range of a few hundred dollars for standard designs. Scintillator-photomultiplier combinations range from about a thousand to several thousand dollars, depending on size and resolution. Room-temperature semiconductor detectors range from less than one hundred dollars for small, low-resolution devices to over a thousand dollars for large (1 cm^3), high-resolution devices. Pricing of coaxial HPGe detectors is based largely on their gamma ray efficiency, which is specified relative to a 3×3 -in. sodium iodide scintillator at 1.33 MeV. Coaxial detectors are available with relative efficiencies up to about 150 percent with cost in the area of several hundred dollars per percent efficiency. Planar HPGe detectors are normally less expensive than coaxial designs. In either case, the price includes cryostat, dewar, and preamplifier. Cryogenic silicon detectors are available in area up to several tens of square millimeters. Cost ranges to $> \$10,000$, depending on size, performance, and complexity of design.

References

1. G. F. Knoll, *Radiation Detection and Measurement*, New York: John Wiley and Sons, 1979.
2. R. B. Rossi and H. H. Staub, *Ionization Chambers and Counters*, New York: McGraw-Hill, 1949.
3. M. J. Weber, P. Lecoq, R. C. Ruchti, C. Woody, W. M. Yen, and R. Y. Zhu (eds.), *Scintillator and Phosphor Materials*, Vol. 348, Materials Research Society, Pittsburgh, PA, 1994.
4. T. E. Schlesinger and R. B. James (eds.), *Semiconductors for Room-Temperature Nuclear Detector Applications*, Vol. 43, Semiconductors and Semimetals, San Diego, CA: Academic Press, 1995.
5. R. B. James, T. E. Schlesinger, P. Siffert, and L. Franks (eds.), *Semiconductors for Room-Temperature Radiation Detector Applications*, Vol. 302, Materials Research Society, Pittsburgh, PA, 1993.
6. J. Fraden, *AIP Handbook of Modern Sensors*, American Institute of Physics, New York, 1993.
7. M. Cuzin, R. B. James, P. F. Manfredi, and P. Siffert (eds.), *Proceedings of the 9th International Workshop on Room Temperature Semiconductor X- and Gamma-Ray Detectors*, Grenoble, France: Sept. 18–22, 1995, *Nucl. Instru. and Meth.*, 380, 1996.
8. T. E. Bortner, G. S. Hurst, and W. G. Stone, Drift velocities of electrons in some commonly used counting gases, *Rev. Sci. Instru.*, 28(2), 103, 1957.
9. W. J. Price, *Nuclear Radiation Detection*, New York: McGraw-Hill, 1958
10. F. H. Attix and W. C. Roesch, *Radiation Dosimetry*, 2nd Ed., New York: Academic Press, 1966.
11. W. H. Tait, *Radiation Detection*, Boston: Butterworth, 1980.
12. G. N. Whyte, *Principles of Radiation Dosimetry*, New York: John Wiley & Sons, 1959.
13. J. B. Birks, *Theory and Practice of Scintillation Counting*, New York: MacMillan, 1964.
14. J. Markakis, High resolution scintillation spectroscopy with HgI_2 as the photodetector, *Nucl. Instru. Meth.*, A263, 499, 1988.
15. R. N. Hall, Chemical impurities and lattice defects in high-purity germanium, *IEEE Trans. Nucl. Sci.*, 260, NS-21, 260–272, 1974.
16. E. E. Haller, W. L. Hansen, and F. S. Goulding, Physics of ultra-pure germanium, *Adv. In Physics* 30(1), 93–138, 1981.
17. W. G. Pfann, *Zone Melting*, New York: John Wiley & Sons, 1966.
18. G. K. Teal, and J. B. Little, Growth of germanium single crystals, *Phys. Rev.*, 78, 647, 1950.
19. R. H. Pehl, E. E. Haller, and R. C. Cordi, Operational characteristics of germanium detectors at higher temperatures, *IEEE Trans. Nucl. Sci.*, NS-20, 494, 1973.
20. L. S. Darken and C. E. Cox, High-purity germanium detector, p. 23, in *Semiconductors for Room-Temperature Nuclear Detector Applications*, New York, Academic Press, 1995.
21. R. H. Pehl, N. W. Madden, J. H. Elliott, T. W. Raudorf, R. C. Trammell, and L. S. Darken, Jr., Radiation damage resistance of reverse electrode GE coaxial detectors, *IEEE Trans. Nucl. Sci.*, NS-26, 321, 1979.

22. *IEEE Test Procedures for Germanium Detectors for Ionizing Radiation*, ANSI/IEEE Standard 325–1989.
23. R. H. Pehl and F. S. Goulding, Recent observations on the fano factor in germanium, *Nucl. Instru. Meth.*, 81, 329–330, 1970.
24. J. Lacer, E. E. Haller, and R. C. Cordi, Entrance windows in germanium low-energy X-ray detectors, *IEEE Trans. Nucl. Sci.*, NS-24, 53, 1977.
25. C. E. Cox, B. G. Lowe, and R. Sareen, Small area high purity germanium detectors for use in the energy range 100 eV to 100 keV, *IEEE Trans. Nucl. Sci.*, 35, 28, 1988.
26. E. M. Pell, Ion drift in an *n-p* junction, *J. Appl. Phys.*, 31, 291, 1960.
27. J. Kemmer, Fabrication of low noise silicon radiation detectors by the planar process, *Nucl. Instru. Meth.*, 169, 499–502, 1980.
28. J. Kemmer and G. Lutz, New detector concepts, *Nucl. Instru. Meth.*, A235, 365–377, 1987.
29. G. D. Alkhazov, A. P. Komar, and A. Vorob'ev, Ionizing fluctuations and resolution of ionization chambers and semiconductor detectors, *Nucl. Instru. Meth.*, 48, 1–12, 1967.
30. J. Kemmer, P. Burger, R. Henck, and E. Heijne, Performance and applications of passivated ion-implanted silicon detectors, *IEEE Trans. Nucl. Sci.*, NS-29, 733, 1982.
31. T. Dubbs, S. Kashigin, M. Kratzer, W. Kroeger, T. Pulliam, H. F.-W. Sadrozinski, E. Spencer, R. Wichmann, M. Wilder, W. Bialas, W. Daabrowski, Y. Unno, and T. Oshugi, Noise determination in silicon micro strips, *IEEE Trans. Nucl. Sci.*, 42, 1119, 1996.
32. Y. Saitoh, T. Akamine, M. Inoue, J. Yamanaka, K. Kadoi, R. Takano, Y. Kojima, S. Miyahara, M. Kamiaya, H. Ikeda, T. Matsuda, T. Tsuboyama, H. Ozaki, M. Tanaka, H. Iwasaki, J. Haba, Y. Higashi, Y. Yamada, S. Okuno, S. Avrillon, T. Nemota, I. Fulunishi, and Y. Asano, Fabrication of a double-sided silicon microstrip detector with an ONO capacitor dielectric film, *IEEE Trans. Nucl. Sci.*, 43, 1123, 1996.
33. P. Chochula, V. Cindro, R. Jeraj, S. Macek, D. Zontar, M. Krammer, H. Pernegger, M. Pernicka, and C. Mariotti, Readout of a Si strip detector with 200 μm pitch, *Nucl. Instru. Meth.*, A377, 409–411, 1996.
34. T. I. Westgaard, B. S. Avset, N. N. Ahmed, and L. Eversen, Radiation hardness of punch-through and FET biased silicon microstrip detectors, *Nucl. Instru. Meth.*, A377, 429–434, 1996.
35. E. Gatti and P. Rehak, Semiconductor drift chamber—an application of a novel charge transport scheme, *Nucl. Instru. Meth.*, 225, 608–614, 1984.
36. P. Rehak, J. Walton, E. Gatti, A. Longoni, M. Sampietro, J. Kemmer, H. Dietl, P. Holl, R. Klanner, G. Lutz, A. Wylie, and H. Becker, Progress in semiconductor drift detectors, *Nucl. Instru. Meth.*, A248, 367–378, 1986.
37. P. Lechner, S. Eckbauer, R. Hartman, S. Krisch, D. Hauff, R. Richter, H. Soltau, L. Struder, C. Fiorini, E. Gatti, A. Longoni, and M. Sampietro, Silicon drift detectors for high resolution room temperature X-ray spectroscopy, *Nucl. Instru. Meth.*, A377, 346–351, 1996.
38. H. Brauning, R. Danner, D. Hauff, P. Lechner, G. Lutz, N. Meidinger, E. Pinotti, C. Reppin, L. Struder, and J. Trumper, First results with the *pn*-CCD detector system for the XMM satellite mission, *Nucl. Instru. Meth.*, 129, 1993.
39. K. Misiakos and S. Kavadias, A pixel segmented silicon strip detector for ultra fast shaping at low noise and low power consumption, *IEEE Trans. Nucl. Sci.*, 43, 1102, 1996.
40. E. Beauville, C. Cork, T. Earnest, W. Mar, J. Millaud, D. Nygen, H. Padmore, B. Turko, G. Zizka, P. Datte, and N.H. Xuong, A 2D smart pixel detector for time resolved protein crystallography, *IEEE Trans. Nucl. Sci.*, 43(3), 1243, 1996.
41. H. K. Hecht, Zum mechanismen des lichtelektrischen primarstromes in isolierenden kristallen, *Z Phys.*, 77, 235–245, 1932.
42. J. S. Iwanczyk, B. E. Patt, Y. J. Wang, and A. K. Khusainov, Comparison of HgI₂, CdTe, and Si (*p-i-n*) X-ray detectors, *Nucl. Instru. Meth.*, A380, 186–192, 1996.
43. V. Gerrish, private communication, 1995.

44. R. Olsen, R. B. James, A. Antolak, C. Wang, *Proceedings of the 1994 International Nuclear Materials Management Conference*, 23, 589, 1994.
45. B. E. Patt, J. S. Iwaczyk, G. Vikelis, and Y. J. Wang, New gamma-ray detector structures for electron only charge carrier collection utilizing high-Z compound semiconductors, *Nucl. Instr. Meth.*, A380, 276–281, 1996.
46. P. N. Luke, Electrode configuration and energy resolution in gamma-ray detectors, *Nucl. Instr. Meth.*, A380, 232–237, 1996.